Structural and Mechanistic Insights into Unusual Thiol Disulfide Oxidoreductase

Edwige B Garcin, Olivier Bornet, Latifa Elantak, Nicolas Vita, Laetitia Pieulle, Francoise Guerlesquin, Corinne Sebban-Kreuzer

▶ **To cite this version:**

Edwige B Garcin, Olivier Bornet, Latifa Elantak, Nicolas Vita, Laetitia Pieulle, et al.. Structural and Mechanistic Insights into Unusual Thiol Disulfide Oxidoreductase. Journal of Biological Chemistry, 2012, 287 (3), pp.1688-1697. ⟨10.1074/jbc.m111.288316⟩. ⟨hal-02018153⟩

HAL Id: hal-02018153

https://hal.science/hal-02018153v1

Submitted on 13 Feb 2019

HAL is a multi-disciplinary open access archive for the deposit and dissemination of scientific research documents, whether they are published or not. The documents may come from teaching and research institutions in France or abroad, or from public or private research centers.

L'archive ouverte pluridisciplinaire **HAL**, est destinée au dépôt et à la diffusion de documents scientifiques de niveau recherche, publiés ou non, émanant des établissements d'enseignement et de recherche français ou étrangers, des laboratoires publics ou privés.

HAL Authorization

THE JOURNAL OF BIOLOGICAL CHEMISTRY VOL. 287, NO. 3, pp. 1688–1697, January 13, 2012
© 2012 by The American Society for Biochemistry and Molecular Biology, Inc. Published in the U.S.A.

Structural and Mechanistic Insights into Unusual Thiol Disulfide Oxidoreductase[S]

Received for publication, August 1, 2011, and in revised form, November 20, 2011 Published, JBC Papers in Press, November 28, 2011, DOI 10.1074/jbc.M111.288316

Edwige B. Garcin, Olivier Bornet, Latifa Elantak, Nicolas Vita, Laetitia Pieulle, Françoise Guerlesquin, and Corinne Sebban-Kreuzer[1]

From the IMR, IFR88, CNRS, Aix-Marseille Université, Marseille 13402, France

Background: TDOR are ubiquitous and catalyze important cell redox reactions.
Results: Dtrx presents atypical physicochemical properties and a positive surface around its active site, suggesting a specificity for it(s) substrate(s).
Conclusion: Active site histidine plays an important role in the molecular mechanism of Dtrx catalysis.
Significance: Structural and functional studies of such atypical systems will give new insights into the TDOR catalytic mechanism.

Cytoplasmic desulfothioredoxin (Dtrx) from the anaerobe *Desulfovibrio vulgaris* Hildenborough has been identified as a new member of the thiol disulfide oxidoreductase family. The active site of Dtrx contains a particular consensus sequence, CPHC, never seen in the cytoplasmic thioredoxins and generally found in periplasmic oxidases. Unlike canonical thioredoxins (Trx), Dtrx does not present any disulfide reductase activity, but it presents instead an unusual disulfide isomerase activity. We have used NMR spectroscopy to gain insights into the structure and the catalytic mechanism of this unusual Dtrx. The redox potential of Dtrx (−181 mV) is significantly less reducing than that of canonical Trx. A pH dependence study allowed the determination of the pK_a of all protonable residues, including the cysteine and histidine residues. Thus, the pK_a values for the thiol group of Cys^{31} and Cys^{34} are 4.8 and 11.3, respectively. The His^{33} pK_a value, experimentally determined for the first time, differs notably as a function of the redox states, 7.2 for the reduced state and 4.6 for the oxidized state. These data suggest an important role for His^{33} in the molecular mechanism of Dtrx catalysis that is confirmed by the properties of mutant DtrxH33G protein. The NMR structure of Dtrx shows a different charge repartition compared with canonical Trx. The results presented are likely indicative of the involvement of this protein in the catalysis of substrates specific of the anaerobe cytoplasm of *Dv*H. The study of Dtrx is an important step toward revealing the molecular details of the thiol-disulfide oxidoreductase catalytic mechanism.

Thiol/disulfide oxidoreductases (TDOR)[2] are ubiquitous in prokaryotes and eukaryotes and catalyze important redox reactions in the cell (1, 2). All of the members of this family share the thioredoxin fold consisting of a central β-sheet surrounded by four α-helices and an active site with two conserved cysteine residues that specify the biological activity of the protein (3). Despite these similarities, thiol/disulfide oxidoreductases can be subdivided according to their cellular location. Although the cytoplasmic members of this family such as thioredoxin (Trx) and glutaredoxin catalyze the reduction of disulfide bonds, the members of oxidizing cellular compartments, such as protein-disulfide isomerase (PDI) from the endoplasmic reticulum and disulfide bond proteins DsbA and DsbC from the bacterial periplasm, are catalysts of disulfide bond formation during folding of secreted proteins.

The *CXXC* active site of these proteins is essential for TDOR activity. The sequence of the *XX* dipeptide located between the cysteines in the active site motif is very important in controlling the redox properties of the protein (5–7). Within each subgroup the active site contains a conserved consensus sequence (Trx, CGPC; glutaredoxin, CPYC; PDI, CGHC; DsbA, CPHC; DsbC, CGYC).

In all thioredoxin-like proteins, the reactivity is influenced by the pK_a value of the first active site cysteine residue and by the redox potential ($E^{0\prime}$) of the disulfide bond. There is a remarkable correlation between the standard redox potential of these enzymes and their physiological role; indeed the members with the lowest redox potentials catalyze reducing processes *in vivo* (Trx, −270 mV (4); and glutaredoxin, −233 to −198 mV (5)), whereas the protein folding catalysts are strong oxidizing agents (PDI, −175 to −147 mV (6, 7); and DsbA, −163 to −80 mV (8)). Exceptions are the thioredoxin-like proteins anchored to the inner bacterial membrane. As an example, TlpA (thioredoxin-like protein A) from *Bradyrhizobium japonicum* exhibits a low redox potential (−259 mV) despite its periplasmic orientation and is required for cytochrome aa_3 maturation (9). However, no high redox potential has ever been reported for cytoplasmic TDOR.

Thioredoxins are a group of small (12 kDa) proteins. They have been characterized from various prokaryotic and eukaryotic organisms (10). The thioredoxin system comprises a thioredoxin with the active site consensus sequence WCGPC

[S] This article contains supplemental Table S1 and Figs. S1–S6.
The atomic coordinates and structure factors (codes 2L6D and 2L6C) have been deposited in the Protein Data Bank, Research Collaboratory for Structural Bioinformatics, Rutgers University, New Brunswick, NJ (http://www.rcsb.org/).

[1] To whom correspondence should be addressed. Tel.: 33-4-91-16-44-53; Fax: 33-4-91-16-45-40; E-mail: Corinne.kreuzer@ifr88.cnrs-mrs.fr.

[2] The abbreviations used are: TDOR, thiol-disulfide oxidoreductases; Dsb, disulfide bond protein; Dtrx, desulfothioredoxin; PDI, protein-disulfide isomerase; Trx, thioredoxin; HSQC, heteronuclear single quantum coherence.

Downloaded from http://www.jbc.org/ at CNRS on December 12, 2018

(Trx), a thioredoxin reductase, and NADPH. The molecular catalytic mechanism actually proposed for the reduction of the oxidized substrate proteins by the canonical Trx involves a bimolecular nucleophilic substitution reaction. The reaction starts with a nucleophilic attack of the N-terminal thiol of the W*CXX*C motif on the disulfide bond of the target protein, releasing a free thiol and forming a mixed disulfide between Trx and its substrate. In the second step, the C-terminal thiol must be activated as a thiolate to allow the dissociation of the complex. For deprotonation of the C-terminal thiol, one hypothesis involves a conserved aspartate residue (11). Recently, it was suggested that when the N-terminal thiolate of Trx attacks its substrate disulfide to form a mixed disulfide complex, the leaving thiol group deprotonates the thiol of the C-terminal active site of Trx (12). Finally another hypothesis proposes that the cysteine is activated for its nucleophilic attack by hydrogen bonds between this residue and the backbone amide of the active site tryptophan (13).

In *Desulfovibrio vulgaris* Hildenborough, a Gram-negative sulfate-reducing bacteria, two cytoplasmic thioredoxin systems have been identified (14). The Trx1/TR1 system contains the ubiquitous thioredoxin with the active site consensus sequence WCGPC. The second system contains an atypical thioredoxin with a CPHC sequence at the active site identical to the DsbA motif and an unconventional thioredoxin reductase that uses preferentially NADH (14). The presence of these atypical proteins being restricted to *Desulfovibrio* organisms, they have been named desulfothioredoxin (Dtrx) and desulfothioredoxin reductase (15).

In this work, we have determined the disulfide isomerase and reductase activities and redox properties for the cytoplasmic CPHC active site. We have solved the structure of Dtrx and investigated the catalytic mechanism of this atypical enzyme. We identified important structural differences between Dtrx and the canonical bacterial Trx1 in the areas surrounding the catalytic sites.

EXPERIMENTAL PROCEDURES

Protein Production—The encoding sequence (DVU378) of desulfothioredoxin from *D. vulgaris* Hildenborough was cloned into expression vector pJF119-EH for production of a His-tagged protein at its C terminus.

pJF119-EH Dtrx plasmid with the desulfothioredoxin wild-type gene was used as DNA template in two separate PCRs to introduce the H33G mutation with two pair of primers (an internal mutagenic forward primer (H1: 5′-CCTGTGC-CCGGGCTGCAAGAAC-3′) and an external reverse primer (C2: 5′-GCTTCTGCGTTCTGATTTAATCTG-3′); and an internal mutagenic reverse primer (H2: 5′-GTTCTTGCAGC-CCGGGCACAGG-3′) and an external forward primer (C1: 5′-GCAGAAACGTGGCTGGCCTGG-3′)). The two PCR-purified fragments were mixed, denatured, and extended. The product was then amplified in a third PCR using C1 and C2 primers. The resulting fragments were digested with BamHI and EcoRI and cloned into the pJF119-EH vector.

Transformed *Escherichia coli* TG1 cells were grown in a M9 minimal medium containing $^{15}NH_4Cl$ (1 g/liter) and [^{13}C]glucose (2 g/liter) as the sole nitrogen and carbon sources. Protein purification was achieved using nickel-nitrilotriacetic acid affinity chromatography and imidazole gradient (20–500 mM) in 500 mM NaCl and 100 mM phosphate buffer at pH 8. The purity of the protein sample was checked by SDS-PAGE.

NMR Spectroscopy—NMR spectra were recorded on Bruker Avance III 600 MHz spectrometer equipped with a TCI cryoprobe or a Bruker Avance III 500 MHz spectrometer equipped with a TXI probe. All of the experiments were carried out at 298 K. The spectra were processed using Topspin (Bruker).

Activity Assay—The ability of Trx1 and Dtrx, wild-type and mutant, to catalyze insulin reduction in the presence of DTT was determined as previously described (16). The reaction mixtures were prepared in cuvettes containing 130 μM insulin, 5 μM protein catalyst in different 0.1 M buffers (pH 4.22, 6.3, 7.06, 7.52, 8.11, and 8.98), and 2.5 mM EDTA. For Dtrx, we also used a 20 μM concentration. The reactions were started with the addition of 1 mM DTT. The rate of precipitation was monitored by recording the increased turbidity of the reaction mixture, which was measured at 650 nm every 30 s at 33 °C and using an Uvikon spectrophotometer. The noncatalyzed reduction of insulin by DTT was monitored in a control reaction.

An *in vitro* assay involving refolding of scrambled RNase A was used to monitor the oxidase activity of Trx1, Dtrx, DtrxH33G mutant, and DsbC (ATGen, Seongnam-SI, South Korea) (17). Disulfide-scrambled RNase A was produced by incubating 30 mg of native RNase A (Sigma) overnight at room temperature in 50 mM Tris-HCl, pH 8.5, in the presence of 6 M guanidinium chloride and 130 mM DTT. After acidifying the solution (addition of 1 μl of 11 M acetic acid), the DTT was removed by passing the sample through a desalting column. The RNase A concentration was then determined at 280 nm. The fully reduced sample was diluted to 0.5 mg·ml^{-1} in water at pH 6.7. Reshuffling of scrambled RNase A (15 μM) was carried out by incubation 15 min in 5 mM potassium phosphate buffer, pH 7.0, with 60 μM protein sample. The RNase activity was assayed by analysis of RNA hydrolysis after 30 min of reaction by NMR. For the determination of a percentage of the RNase A activity, the mean intensity of several isolated peaks in one-dimensional NMR spectrum of RNA was used relative to the RNA spectrum in the presence of native RNase A. The RNA spectrum in the presence of ScRNase A is used as blank.

An *in vivo* assay involving refolding of PalB (lipase B from *Pseudozyma antarctica*) was used to monitor the isomerase activity of Trx1 and Dtrx. DNA fragments containing the leaderless *palB* gene were PCR-amplified using PrimeSTAR HS DNA polymerase (TAKARA), the primer pair (P1/P3 or P2/P3), and *P. antarctica* chromosomal DNA as template. One PCR product was cloned into the restriction sites SacI/XbaI of the pJF119EH vector. The second PCR product was used to obtain by PCR a *palB* fusion construct with Trx1 and Dtrx ORFs and cloned into pJF119EH vector with EcoRI/XbaI (P1, 5′-CCGA-GCTCATGCTACCTTCCGGTTCGGACCCTG-3′; P2, 5′-CGGTAGTGGTTCTGGGCTACCTTCCGGTTCGGACC-3′; and P3, 5′-GCTCTAGATCAGGGGGTGACGATG-CCGGAGC-3′).

Rosetta-gami 2 and TG1 *E. coli* cells were transformed with pJF119EH constructs. The cells were grown in LB medium containing 100 μg/ml ampicillin at 310 K. When the cell density

Downloaded from http://www.jbc.org/ at CNRS on December 12, 2018

reached ~0.8 A_{600}, PalB, DTrx-PalB and Trx1-PalB expressions were induced by the addition of 1 mM isopropyl β-D-thiogalactopyranoside at 37 °C overnight. PalB activity was qualitatively evaluated by the area and the transparency of the halo formed on the tributyrin agar plate (LB agar plate containing 1% emulsified tributyrin). The PalB-producing strains were transferred onto the plate and incubated at room temperature until the halos developed.

Determination of Redox Potential—For NMR spectroscopy, two samples of 0.3 mM Dtrx and 0.6 mM DtrxH33G were dialyzed against 50 mM potassium phosphate buffer, pH 7.0, supplemented with 4 mM GSSG. Dtrx and DtrxH33G were titrated with GSH in the ranges 0–30 and 0–90 mM, respectively. ^{15}N-^{1}H HSQC spectra were recorded upon titration with reduced or oxidized glutathione. For the determination of the redox potential, the intensities of several isolated peaks in each NMR spectrum were obtained from Topspin and plotted *versus* the half-cell potential of glutathione. Redox potential was obtained by fitting the experimental curve against a sigmoidal decay (logistic) function. Subsequently, $E^{0'}$ values obtained for individual peaks were averaged.

The half-cell potential of glutathione for the reaction GSSG + $2H^+ + 2e^- \rightarrow 2GSH$ was calculated according to the Nernst equation,

$$E_{hc}(mV) = E^{0'} - \frac{RT}{nF} \cdot \ln\left(\frac{[GSH]^2}{[GSSG]}\right) \cdot 10^3 \qquad \text{(Eq. 1)}$$

where R is the universal gas constant (8.3145 J K^{-1} mol^{-1}), T is the temperature in Kelvin, $n = 2$ for the two-electron reduction, and F is the Faraday constant ($9.6485 \cdot 10^4$ C mol^{-1}).

The standard (midpoint) potential ($E^{0'}$) was defined as the potential at 50% of the maximal resonance intensity. For the GSH/GSSG pair, $E^{0'}$ was previously determined to be −240 mV at 298 K, pH 7.0 (5).

pK_a Determination—NMR experiments were carried out on samples containing 1 mM concentration protein with and without DTT. The behavior of the ^{13}C chemical shifts in the protein as a function of pH was monitored using a two-dimensional CBCACO experiment (18). Assignment of these chemical shifts was verified for each pH using a three-dimensional HNCO experiment. Chemical shift values as a function of pH were analyzed according to a single titration curve as shown in Equation 2 (19),

$$\delta = \delta_{HA} - \left(\frac{(\delta_{HA} - \delta_A)}{(1 + 10^{n(pK_a - pH)})}\right) \qquad \text{(Eq. 2)}$$

where δ is the observed chemical shift at a given pH, δ_{HA} and δ_A are the chemical shifts for the various protonated forms of the protein, and n is the number of protons transferred.

Structure Calculation—The NMR sample contained 1 mM protein concentration (90% H_2O, 10% D_2O) in 100 mM NaCl, 50 mM phosphate buffer, pH 5.5. For experiments regarding the reduced form of the protein, the intramolecular disulfide bond of Dtrx was reduced by adding DTT to a final concentration of 10 mM, under argon atmosphere. The spectra were analyzed with CARA (20) on the basis of the previously published backbone amide and side chain resonances assignment (15). The approximate interproton distances were obtained from the two-dimensional NOESY, ^{13}C NOESY-HSQC, and ^{15}N NOESY-HSQC spectra. For structure calculations, 1846 restraints were used for the reduced Dtrx and 2108 restraints for the oxidized form. The mixing time was 150 ms for all of the NOESY experiments. A series of ^{15}N-^{1}H HSQC spectra was acquired on a sample freshly dissolved in $^{2}H_2O$ to identify the slowly exchanging amides. Amides that had not exchanged after 1 h were located in regions of defined secondary structures, based on the NOE data, and were restrained to form HN-CO hydrogen bonds, using the distance restraints of 2.7–3.0 Å for O-N and 1.8–2.0 Å for O-HN, respectively. For structure calculations, 48 restraints were used for backbone hydrogen bonds for the reduced Dtrx and 70 restraints for the oxidized form. 156 backbone φ and ψ dihedral supplemental restraints were derived from TALOS using as input the ^{1}Hα, ^{13}Cα, ^{13}Cβ, ^{13}C′, and ^{15}N chemical shifts (21).

Input data and structure calculation statistics are summarized in supplemental Table S1. The accuracy of the NMR models could be assessed based on the criteria for successful structure calculation using the program CYANA (25). The 20 lowest energy (total energy) structures chosen for the final structural ensemble were subjected each to restrained molecular dynamics using the Amber 4.1 force field within the SANDER module of Amber 10. The water molecules were stripped off, and energy terms were calculated for the protein using AMBER. The nonbonded interaction cutoff was 15 Å for the restrained MD runs. The structure coordinates have been deposited in the Protein Data Bank under accession numbers 2L6D and 2L6C for the reduced and oxidized Dtrx, respectively.

RESULTS

Dtrx Activities—The particular CPHC sequence at the Dtrx active site opens the question of the enzymatic function of this protein. Therefore, we have examined the redox activity of this atypical protein using *in vitro* assays.

First, we used the insulin reduction assay at different pH levels. In this assay, oxidoreductase enzymes reduced the interchain disulfide bond of insulin, causing precipitation of the insoluble insulin β-chain. Precipitation was monitored as an increase in absorbance at 650 nm. We have realized this assay with both Trx1 and Dtrx at pH ranging from 4 to 9. As expected, we found that Trx1 is as active as *E. coli* Trx. Surprisingly, Dtrx is unable to reduce insulin even at concentrations 10 times greater (Fig. 1*A*). It is the first time that a thioredoxin-related protein does not show activity in insulin assay. However, Dtrx demonstrates a reductase activity on artificial substrate as dithiobis(nitrobenzoic acid) (14).

We investigated the ability of Dtrx to catalyze disulfide isomerization. We measured the capacity of Dtrx to isomerize, or shuffle, incorrect disulfides of scrambled RNase A at pH 7 (Fig. 1*B*). After incubation of scrambled RNase A and Dtrx (molar ratio 1:4), we have followed the RNase activity by observing the digestion of RNA using ^{1}H NMR spectra (supplemental Fig. S1). We have used the DsbC isomerase as a positive control. We found that, under our experimental conditions, after 15 min of incubation, the sample containing Dtrx and Trx1 yielded 40 and 5% active RNase A, respectively. DsbC

Downloaded from http://www.jbc.org/ at CNRS on December 12, 2018

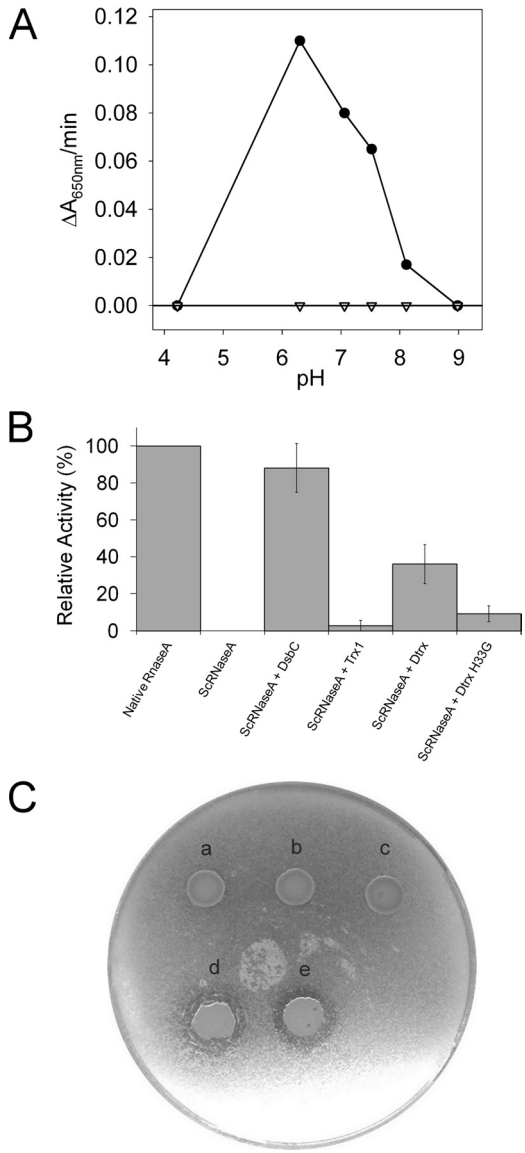

FIGURE 1. **Dtrx activities.** *A*, insulin reduction assay by Trx1 and Dtrx as a function of pH. The disulfide reductase activity was determined by using the insulin reduction assay. The assay was performed at 306 K with 2 μM Dtrx (*triangle*) or 2 μM Trx1 (*black circle*). The catalyzed reduction of insulin (100 μM) was followed by measuring an increase in absorbance at 650 nm and evaluated at different pH levels: 4.22, 6.3, 7.06, 7.52, 8.11, and 8.98. The absorbance caused by the nonenzymatic insulin reduction by DTT (1 mM) is substracted. *B*, scrambled RNase A (*ScRNase*) refolding assay: yield of RNase A activity of native RNase A and reshuffling of ScRNase A after incubation with DsbC, Trx1, Dtrx, and Dtrx H33G mutant. For the determination of a percentage of the RNase A activity, the mean intensity of several isolated peaks in RNA spectrum was used relative to the RNA spectrum in the presence of native RNase A. The RNA spectrum in presence of ScRNase A is used as blank. The error analysis of the data points was performed using Excel software. *C*, study of *in vivo* activity. Qualitative visualization of PalB activity using tributyrin plate for recombinant *E. coli* TG1 and Rosetta-gami as host cells. Different expression systems were observed: pJF119EH PalB (*a*), pJF119EH Dtrx-PalB (*b*), pJF119EH Trx1-PalB (*c*) in *E. coli* TG1 and pJF119EH PalB (*d*) and pJF119EH Dtrx-PalB (*e*) in *E. coli* Rosetta-gami.

yielded 85% active RNase A. The weak activity of Trx1 is similar to *E. coli* Trx1, and Dtrx disulfide isomerase activity is comparable with that of *E. coli* DsbA oxidase (22).

To verify the *in vivo* disulfide isomerase activity of Dtrx, we have explored the functional expression of PalB in the cytoplasm of *E. coli* using fusion tag techniques (23). Indeed, PalB has three intramolecular disulfide bonds potentially associated with its folding process and required for developing the bioactivity. The fusion tag technique was explored by constructing two PalB fusions, Trx1 and Dtrx tag. We have compared the expression performance using *E. coli* TG1 and Rosetta-gami strains having a reducing and oxidizing cytoplasm, respectively, as host cells. PalB activity was qualitatively evaluated by the area and transparency of the halo formed on the tributyrin agar plate (Fig. 1*C*). No visible halos developed for Dtrx-PalB fusion. Contrary to DsbA, Dtrx was not able to enhance PalB folding in the *E. coli* cytoplasm by disulfide bond formation (23).

Dtrx Redox Potential—The next step of our study was to compare the redox potential of Dtrx and canonical Trx. The measurement of the redox potential of Dtrx was obtained by ^{15}N-^{1}H HSQC NMR experiments (15). We utilized GSH and GSSG as the redox couple, which has a standard potential of −240 mV at pH 7.0 and 298 K (5). The intensities of the NH resonances of the oxidized form of Dtrx decreased upon the addition of reduced glutathione. At the same time, the intensities of the NH resonances of the reduced form increased. The measurement of the NMR signal intensities resulted in a sigmoidal transition curve. Several chemical shift changes associated with the reduction of the catalytic cysteines of the protein were observed (supplemental Fig. S2). Sigmoidal curves were fitted successfully for the Cys^{34} resonances (Fig. 2). The redox potential for the cysteines of the active site at pH 7.0 was −181.3 ± 1.2 mV. In conclusion, this value indicated that Dtrx was more oxidizing than canonical Trx (−270 mV).

pK_a of Dtrx Protonable Residues—Because there is generally a correlation between the redox potential of the active site and the pK_a of the cysteine residues, we have investigated the pK_a of all the residues of Dtrx. The knowledge of the protonation state for the residues involved in the reaction mechanism is highly important (28, 29), but the pK_a values are not always easy to determine experimentally for all residues (19). This is the first time that a proton-less NMR spectrum (CBCACO) (Fig. 3*A*) was used to follow the pH dependence of $^{13}C\beta$ chemical shift of all residues. In the reduced form, the titration curves in Fig. 3*B* revealed pK_a values of 4.8 and 11.3 for the thiol group of Cys^{31} and Cys^{34} residues, respectively. These values were different from those already reported for canonical Trx: 7.5 for the first cysteine and 9.5 for the second (11). The pK_a of the active cysteine thiol group reflected the stabilization of the thiolate anion. To understand this peculiar property and get some insights into the Dtrx catalytic mechanism, we have determined the pK_a value of all protonable residues in the protein (supplemental Fig. S3). Only the pK_a values of His^{33} from the CPHC active site presented an atypical value and changed strongly between the two redox states of Dtrx, these values being 7.2 and 4.6 for the imidazole group in the reduced and oxidized states, respectively (Fig. 3*C*). It is the first time that pK_a values of the histidine residues found in the CPHC active site motif have been experimentally determined. These data are of particular interest to get precise atomic views of the catalytic site in both redox states of the protein.

Role of His^{33} in Dtrx Catalytic Mechanism—To confirm a potential role of His^{33} in the particular properties of Dtrx, we have mutated this residue into a glycine residue. This mutant

Downloaded from http://www.jbc.org/ at CNRS on December 12, 2018

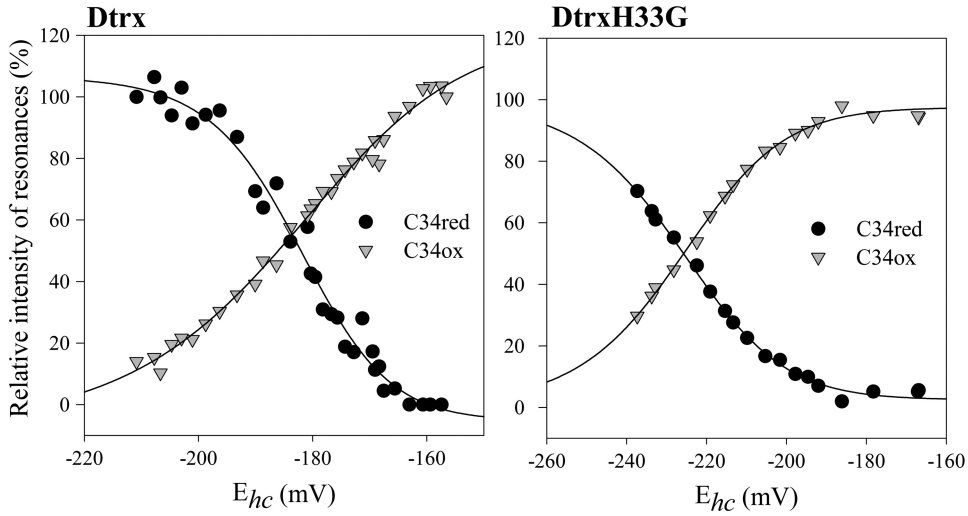

FIGURE 2. **Titration of the redox potential of the disulfide bond of Dtrx and DtrxH33G.** Changes in NMR signal intensities for the NH resonances of Cys^{34} under oxidizing or reducing conditions were reported in the function of half-cell potential of glutathione. *Gray triangles* and *black circles* represent signal intensity in the oxidized and reduced states, respectively. Redox potentials were calculated using the Nernst equation from the ratio of concentrations of reduced and oxidized glutathione. Experimental data were fitted against a sigmoidal decay (logistic) function.

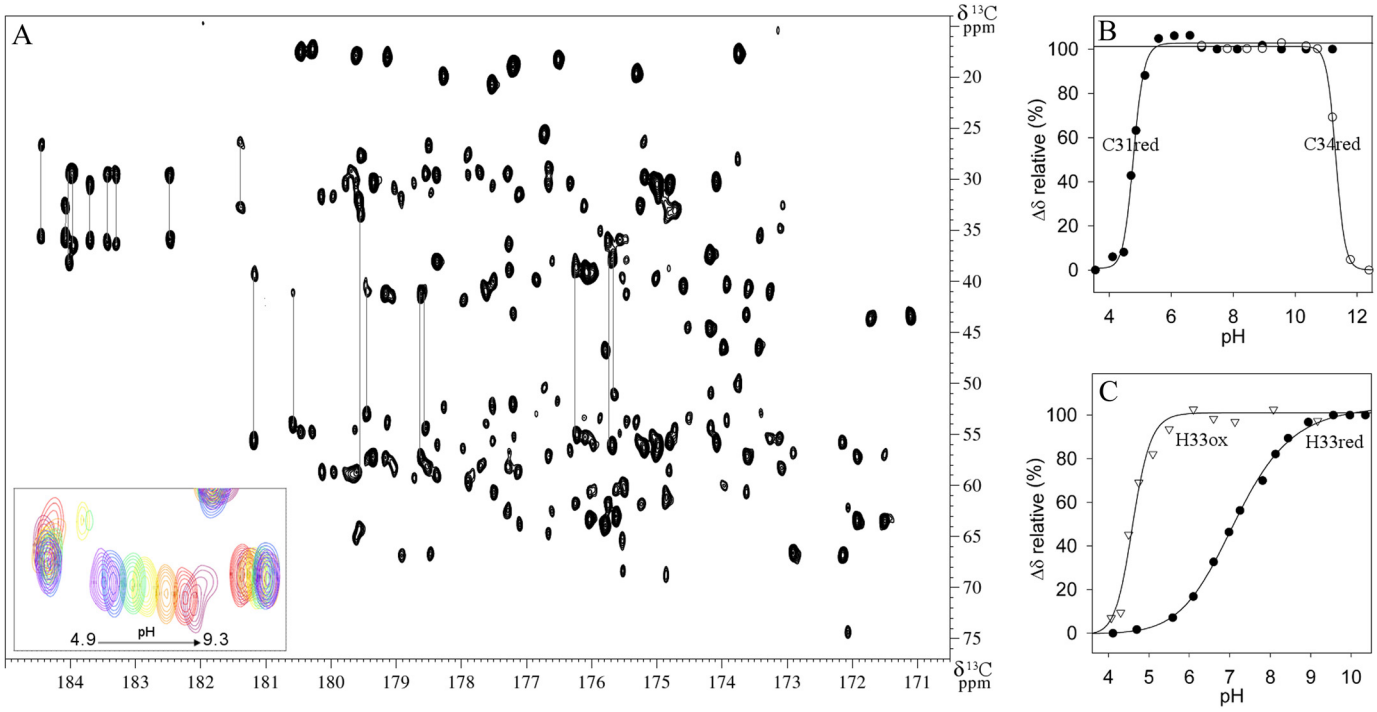

FIGURE 3. **pK_a determination of all Dtrx ionizable residues.** *A*, 600 MHz two-dimensional CBCACO spectrum of reduced Dtrx at 298 K, pH 5.7, showing the cross-peaks for the C_α-CO and C_β-CO of all residues of the protein. Cross-peaks for the C_α-C_γ and C_β-C_γ of Asn and Asp, and for the C_β-C_δ and C_γ-C_δ of Gln and Glu are also visible and connected by *lines*. The *inset* shows a close-up view of the pH-dependent chemical shift variations for the C_β-CO of Asp^{21} (pH 4.9 (*pink*), 5.6 (*red*), 6.1 (*orange*), 6.6 (*yellow*), 7 (*green*), 7.8 (*blue*), and 9.3 (*purple*)). *B*, pK_a determination of the nucleophilic cysteine Cys^{31} (*black circle*) and cysteine Cys^{34} (*white circle*) in the reduced form of Dtrx. *C*, pK_a determination of the histidine His^{33} in the oxidized form (*white triangle*) and reduced form (*black circle*) of Dtrx. The pH-dependent chemical shift variation of the C_β carbons was measured, normalized, and fitted to one apparent pK_a value using the Henderson-Hasselbach equation.

protein (DtrxH33G) was produced and purified as the wild type. The ^1H,^{15}N HSQC spectrum was recorded and compared with the Dtrx spectrum (supplemental Fig. S4). This comparison shows that the mutation does not modify the structure of the protein because only residues close to the mutation undergo weak chemical shift variations. Next, we have determined the activities and the redox potential of the DtrxH33G mutant. In the same experimental conditions as the wild type, we have studied the ability of DtrxH33G to reduce insulin and, like Dtrx, DtrxH33G is unable to reduce insulin. It is thus not the presence of a histidine residue in the active site that induces this particular property of the protein. However, the DtrxH33G mutant shows a loss of the capacity of the protein to isomerize, or shuffle, incorrect disulfides of scrambled RNase A yielding 10% active RNase A only (Fig. 1*B* and supplemental Fig. S1). The histidine residue or the physicochemical properties

Downloaded from http://www.jbc.org/ at CNRS on December 12, 2018

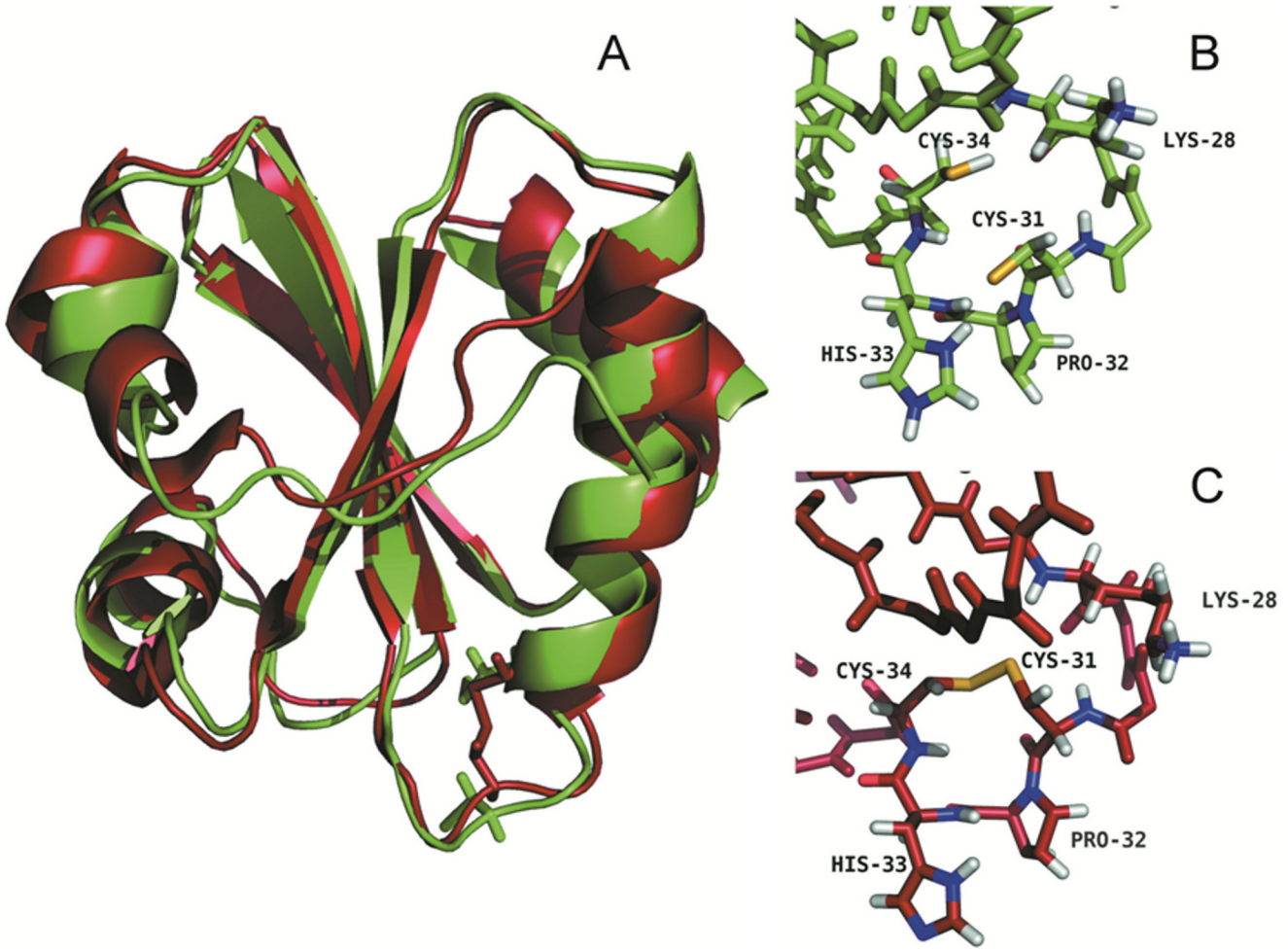

FIGURE 4. **Three-dimensional structure of Dtrx in both redox states.** *A*, overlay of the three-dimensional solution structures of the reduced (*green*) and oxidized (*red*) forms of Dtrx calculated with CYANA (21). The NMR sample contained 1 mM protein concentration (90% H_2O, 10% D_2O) in 100 mM NaCl, 50 mM phosphate buffer, pH 5.7, at 290 K. For reduced Dtrx, the intramolecular disulfide bond was reduced by adding DTT to a final concentration of 10 mM, under argon atmosphere. The Dtrx typical thioredoxin fold is represented in *cartoon*, and the side chains of the cysteine residues are shown in *sticks*. *B*, local conformations of the active site in the reduced form of Dtrx. *C*, local conformations of the active site in the oxidized form of Dtrx. The active site residues Cys^{31}, Pro^{32}, His^{33}, and Cys^{34} are shown and labeled. Sulfur atoms are shown in *yellow*, hydrogen atoms are in *white*, and nitrogen and oxygen atoms are in *blue* and *red*, respectively. The figures were generated using the PyMOL Molecular Graphics System, Version 1.2r3pre, Schrödinger, LLC.

induced by this histidine are essential for Dtrx to catalyze disulfide isomerization. The determination of the redox potential of DtrxH33G shows effectively that His^{33} plays an important role in the Dtrx properties (Fig. 2). The redox potential of the active site cysteines at pH 7.0 for DtrxH33G (−226.4 ± 0.6 mV) is 45 mV more reducing than for the wild type. This value is intermediate between Dtrx (−181.3 mV) and canonical Trx (−270 mV) redox potentials.

Dtrx Structure Analysis—From our studies, the activities, the redox potential, and the pK_a values of Dtrx are significantly different from a canonical Trx. To gain insight into these atypical properties of Dtrx and to propose a molecular catalytic mechanism, we have determined the three-dimensional structure of the enzyme in the two redox states. The reduced and oxidized structures of Dtrx were calculated at pH 5.5 using interproton nOe-derived distance restraints in combination with the dihedral angle (21) and hydrogen bond restraints (supplemental Table S1). We used the pK_a values to define the protonation state of the histidine and cysteine residues in the structure refinement. The resulting ensembles of solutions consisting of the 20 lowest energy structures of the oxidized and the reduced Dtrx are shown in supplemental Fig. S5. These ensembles have a backbone root mean square deviation relative to the average structure of 0.59 ± 0.11 and 0.94 ± 0.15 Å over the polypeptide chain for the oxidized and the reduced Dtrx, respectively. Detailed structure statistics are shown in supplemental Table S1.

Oxidized and reduced Dtrx adopt a typical thioredoxin fold (3). The oxidized form consists of a four-stranded twisted central β-sheet (residues 52–58 (β1), 20–27 (β2), 74–81 (β3), and 83–90 (β4)) surrounded by four α-helices (residues 12–17 (α1), 33–46 (α2), 61–69 (α3), and 93–104 (α4)) (Fig. 4*A*). The overall structure of the reduced Dtrx is similar to the one of the oxidized form. Dtrx displays high three-dimensional similarities to thioredoxins from other species such as *E. coli* Trx1 and the thioredoxin fold domain of other thiol disulfide oxidoreductases such as *E. coli* DsbA and DsbC (30, 31) (supplemental Fig. S6).

With the exception of the disulfide bond, the main structural differences between the two redox states of Dtrx concern the helix α1 because of the number of restraints used in the struc-

Downloaded from http://www.jbc.org/ at CNRS on December 12, 2018

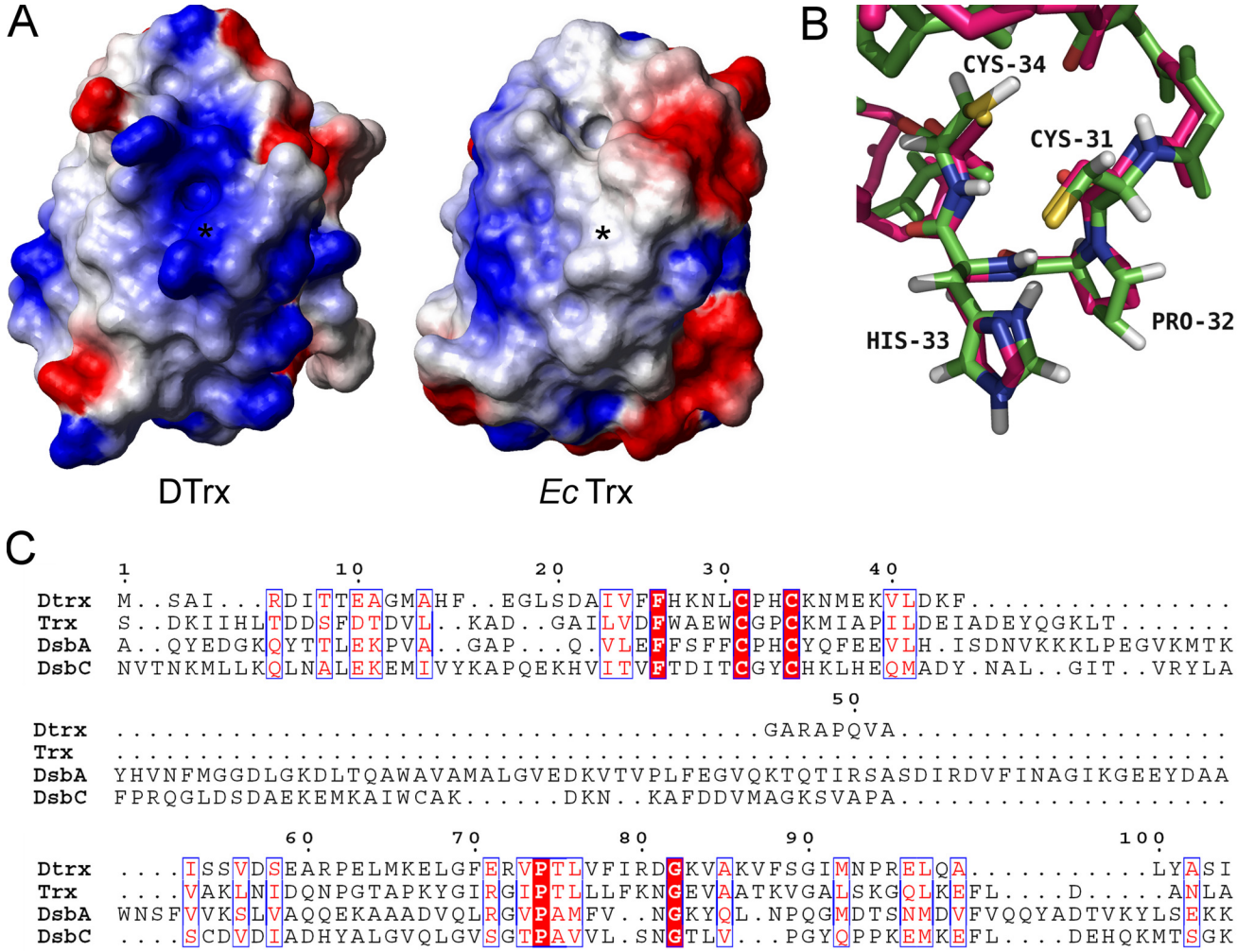

FIGURE 5. **Comparative structural analysis of Dtrx.** *A*, electrostatic surface potential representations of reduced Dtrx and reduced *E. coli* Trx, with *blue* representing basic residues, *red* representing acidic residues, and *white* representing neutral residues. The orientations of Dtrx and Trx are similar. The position of the sulfur atom of the N-terminal cysteine is indicated by a *star*. The hydrophobic patch observed in Trx is not conserved in Dtrx. Surface calculations were made using MolMol. *B*, superimposition of the redox active site of the reduced form of Dtrx (*green*) and *E. coli* DsbA (*pink*) in stick representation. The active site residues are labeled. *C*, sequence alignment of Dtrx, *E. coli* Trx, *E. coli* DsbA, and *E. coli* DsbC. Identical residues are in *red boxes*. Conserved residues are shown in *red*. The alignment was prepared with TCoffee (34) and ESPript (11).

ture calculation. The active site (^{31}CPHC^{34}) of Dtrx is formed by a protruding loop between strand β2 and the N termini of helix α2. Between the two redox states, the cysteine side chain undergoes change in orientation (Fig. 4, *B* and *C*). In the dithiol form, the S atoms are at a mean distance of 4.8 Å. Moreover, a difference in orientation of the histidine His^{33} is observed, positioning the cationic imidazole facing the thiolate anion of the reactive cysteine Cys^{31} at a mean distance of 3.8 Å. In 14 of 20 conformers of the NMR structure, the thiolate anion of Cys^{31} forms two hydrogen bonds with the backbone amide and the HN_δ of His^{33}.

In the reduced Dtrx form, the Cys^{31} side chain is exposed at the protein surface, and the Cys^{34} side chain is pointing toward the interior of the protein, as is the case in the active site of reduced *E. coli* Trx1. The electrostatic surface of Dtrx shows a different charge repartition compared with canonical Trx. Indeed, we observe a positive surface instead of the highly conserved hydrophobic patch found around the canonical active site (Fig. 5, *A* and *B*). The active site of Dtrx is perfectly superimposable to the one of DsbA. Pro^{32} and His^{33} residues occupy the same position when compared with the same residues in DsbA (1A2J) (Fig. 5*C*).

Thioredoxin and DsbA proteins generally contain the conserved residues Asp^{26} and Glu^{24}, respectively, which have been described as involved in the activation of the second cysteine (Fig. 5*D*). As for DsbC, these residues are not found in Dtrx, and no acidic residue is found in the near environment of Cys^{34}. These structural data obtained on Dtrx active site and the striking electrostatic surface potential around the active site strongly suggest a specific function of Dtrx in the anaerobe cytoplasm.

DISCUSSION

Properties of Dtrx—Based on sequence homologies, desulfothioredoxin (Dtrx) from *D. vulgaris* Hildenborough has been identified as a new member of the thioredoxin superfamily. Dtrx contains a particular active site consensus sequence, CPHC, found in the periplasmic DsbA. Dtrx does not show any disulfide reductase activity, being unable to reduce insulin. To date, no protein of the thioredoxin superfamily has shown com-

Downloaded from http://www.jbc.org/ at CNRS on December 12, 2018

parable properties. According to the study of the DtrxH33G mutant, this property is not related to the particular active site of this protein. One explanation is the particular structural properties of Dtrx. The first step of the redox mechanism of Trx is the noncovalent interaction of the oxidized substrate with the hydrophobic surface of the active Trx (10). DsbA contains a helical insertion that forms a hydrophobic patch on the molecular surface, as well as a hydrophobic groove near the active site (32, 33). Rinaldi *et al.* (24) have observed a negative electrostatic surface of *Xylella fastidiosa* DsbA2, indicating that this protein *versus* DsbA has different substrate specificities. It is to be noticed that Dtrx contains a positive surface and no hydrophobic patch around its active site. These differences are the main characteristic of Dtrx structure and may induce a strong specificity for its substrate(s).

An *in vitro* assay involving refolding of scrambled RNase A showed an unusual disulfide isomerase activity of Dtrx. Considering the nature and composition of the sequence in the active site, this activity can be explained. In fact, C*XX*C affects the standard redox potential of the particular proteins. In *E. coli*, the strongest reducing cytosolic Trx (CGPC) has a redox potential of $\Delta E^{0'} = -270$ mV (25), and the strongest oxidizing agents, the periplasmic DsbA (CPHC) and DsbC (CGYC), have a redox potential of $\Delta E^{0'} = -122$ mV (26). The redox potential value of human PDI (CGHC) is an intermediate, $\Delta E^{0'} = -175$ mV (27). The redox potential observed for the cysteine active site of Dtrx at pH 7.0 is −181.3 mV. This characteristic shows that Dtrx is closer to oxidizing enzymes than canonical reductases and even closer to PDI isomerase. This property is in part due to the presence of histidine residue in the active site. Indeed, DtrxH33G lost the ability to catalyze the disulfide isomerization and presents a redox potential closer to disulfide reductases (−226.4 mV).

The pK_a values of 4.8 and 11.3 obtained respectively for the thiol group of Cys^{31} and Cys^{34} residues, are different from those found in all canonical Trx. In *E. coli* Trx1, the pK_a of the thiol group is 7.5 for the first cysteine and 9.5 for the second cysteine in the consensus site (11). The pK_a of this thiol group reflects the stabilization of the thiolate anion of the accessible cysteine residue. Strong stabilization of the thiolate generates a low pK_a value and low stability for the disulfide bond; this phenomenon was observed for Dtrx. The instability of the disulfide bond is characteristic of oxidase or isomerase proteins because it is necessary for their catalytic mechanism (28). In summary, these physicochemical properties of Dtrx are in agreement with the unusual disulfide isomerase activity found in *in vitro* assays for Dtrx.

However, *in vivo*, Dtrx did not present any isomerase activity in the *E. coli* cytoplasm, because it has been observed for DsbA. Indeed, Xu *et al.* (23) showed that a functional expression of PalB in the cytoplasm of *E. coli* appeared to be limited by disulfide bond formation, and a DsbA fusion tag was functional to enhance PalB folding in cytoplasm. Despite the observed *in vitro* disulfide isomerase activity, Dtrx was not able to perform this activity *in vivo* in *E. coli* cytoplasm. Is it a problem of cytoplasmic conditions or of substrate specificity?

The cytoplasm of most organisms is a highly reducing environment, in which protein cysteines are maintained in thiol/thiolate form. However, in extremophile organisms, disulfide bond formation in cytosolic proteins is supposed to increase their thermodynamic stability. Several protein-disulfide oxidoreductases in the disulfide-rich thermophiles were identified and could have dual functions in the cytoplasm, as oxidase and isomerase (29). Therefore we can suppose that oxidase activity could exist in the cytoplasm. Dtrx contains a positive surface and no hydrophobic patch around its active site. These differences are the main characteristic of Dtrx structure and may induce a strong specificity for its substrate(s) and explain the absence of oxidation of lipase *in vivo*, where the ratio Dtrx: lipase is 1:1 in the cell.

Is Dtrx Really a Thioredoxin?—Considering the absence of *in vitro* reductase activity of Dtrx and its oxidizing physicochemical properties (redox potential, pK_a values of the active site), a potential thioredoxin function is questionable. Nevertheless, glutaredoxin, which is a good reducing agent, was also reported to have oxidizing redox properties provided by its low pK_a of the active cysteine (30). Conversely, thioredoxins, which are potent reducing agents, can also act as oxidizing agents under particular conditions. Indeed, *E. coli* thioredoxin can be translocated to the periplasm and then partially replaces the activity of DsbA in promoting the formation of disulfide bonds (31). Thioredoxin can function as a reductase or oxidase or isomerase, mainly depending on the redox environment.

For Dtrx, several aspects support a reductase activity: (i) the three-dimensional structure of Dtrx revealed an identical fold to canonical thioredoxins without a supplementary domain; (ii) the gene DVU_0378 encoding Dtrx is included in a polycistronic unit counting nine other genes, including DVU_0377, which encodes a thioredoxin reductase (desulfothioredoxin reductase) and is able to reduce Dtrx but not any other thioredoxin (14); and (iii) Dtrx has a reductase activity on dithiobis-(nitrobenzoic acid) substrate (14).

Catalytic Mechanism of Dtrx—It is the first time that the pK_a values of the histidine of CPHC active site were determined. These atypical values vary from 7.2 to 4.6 for the reduced to the oxidized Dtrx, respectively.

On the basis of these results, we propose a catalytic mechanism for the reduction of the oxidized substrate by the reduced Dtrx (Fig. 6). The nucleophilic cysteine in the reduced Dtrx is deprotonated by water molecules because of its low pK_a (4.8). The Cys^{31} thiolate of Dtrx nucleophilically attacks a disulfide sulfur atom of the substrate, leading to the formation of the so-called mixed disulfide intermediate in which Dtrx and substrate are covalently bound via a new disulfide bond. Next, the Cys^{34} thiol group of Dtrx is deprotonated. However, the mechanism through which the buried Cys^{34} is deprotonated and activated to perform the intramolecular nucleophilic attack on Cys^{31} is still uncertain in canonical Trx. One hypothesis is that an aspartic acid conserved in all canonical Trx is responsible for this deprotonation (32). It is to be noticed that a double alanine mutation of the conserved Asp^{26} and Lys^{57} in Trx and Glu^{24} and Lys^{58} in DsbA did not change the pK_a of cysteines in both enzymes. These data support the hypothesis that these residues are not involved in the properties of the dithiol active center (33). A second hypothesis involves the thiolate leaving group, which establishes S^-...H-S hydrogen bonds with the thiol

Downloaded from http://www.jbc.org/ at CNRS on December 12, 2018

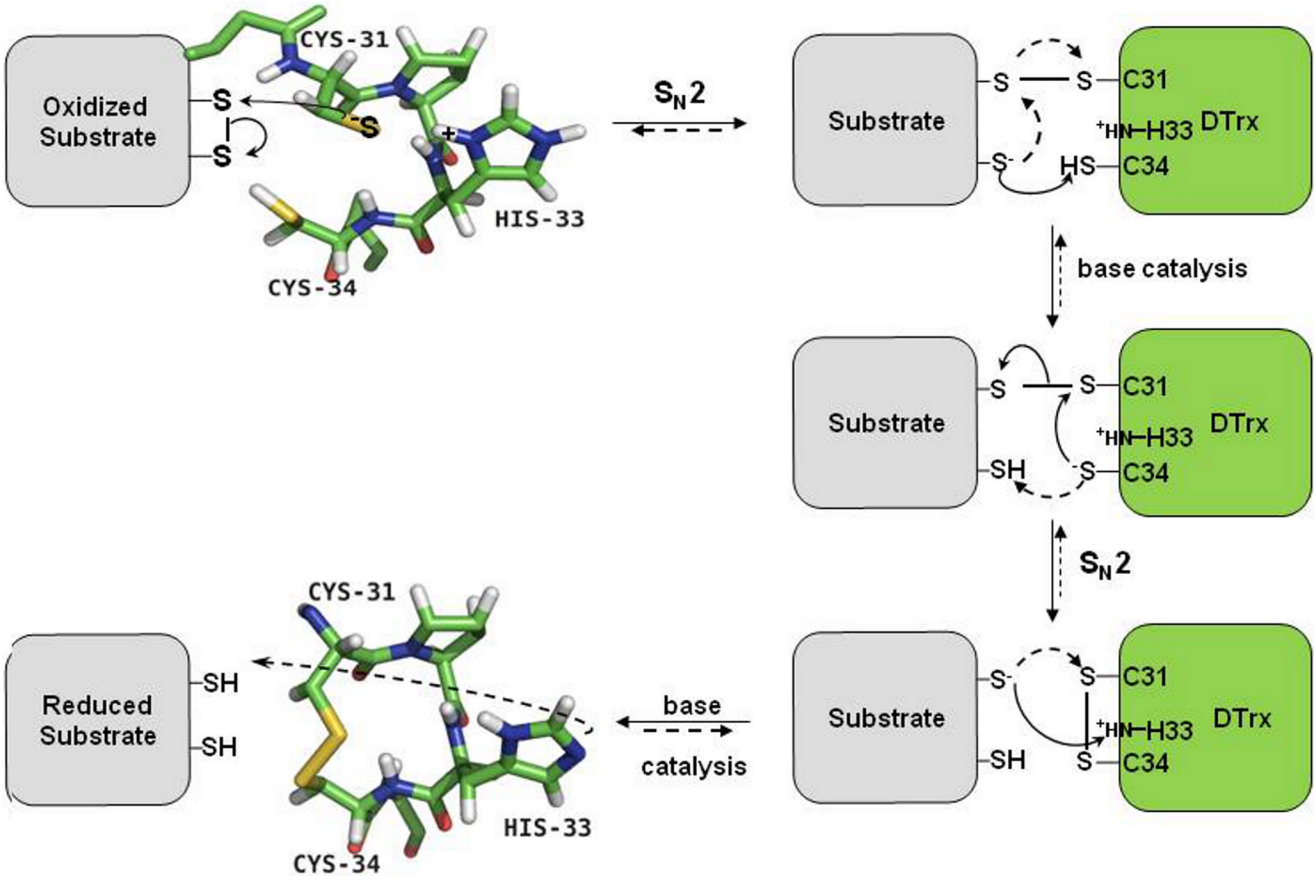

FIGURE 6. **Model of the Dtrx catalytic mechanism.** Substrate reduction (*solid lines*) by Dtrx occurs in four steps. In the first step, the Cys^{31} thiolate of Dtrx nucleophilically attacks sulfur atom of the substrate disulfide. In the second step, the thiolate of the substrate produces a base attack on Cys^{34} sulfur atom. Next, the Cys^{34} thiolate attacks the Cys^{31} sulfur atom involved in the disulfide bond, causing the rupture of the latter. At the same time, the imidazole group of His^{33} is deprotonated by a base attack of the thiolate of the reduced substrate. This reaction produces an oxidized Dtrx and a reduced dithiol substrate. Substrate oxidation (*dotted lines*) by Dtrx occurs in four steps. First, the deprotonated His^{33} produces a base attack on the first cysteine of the substrate. After, this activated cysteine of the substrate nucleophilically attacks the sulfur atom of Cys^{31} of the oxidized Dtrx, leading to the formation of a disulfide-linked complex between Dtrx and the substrate. In the next step, the second cysteine of the substrate is deprotonated probably by the Cys^{34} thiolate of Dtrx and attacks the sulfur atom of the substrate cysteine, which is disulfide-bonded with Cys^{31} of Dtrx. This reaction results in the formation of a disulfide bond in the substrate and the reduction of Dtrx with a protonated His^{33}.

group of the buried cysteines (12). However, the mutation of the second cysteine of the substrate shows a dissociation of the intermolecular complex (13). Finally, in a last hypothesis, the cysteine is proposed to be activated for its nucleophilic attack by hydrogen bonds between this residue and the backbone amides of the tryptophan active site and of the N-terminal cysteine (13). These hydrogen bonds explain the stabilization of thiolate group but not the deprotonation of this group. In Dtrx, the aspartic acid is not conserved, and analysis of pK_a value of all residues does not present any acid group available for the activation of Cys^{34}. Therefore, we centered the mechanism around the second hypothesis where the thiolate of the substrate attacks the Cys^{34} sulfur atom or any acid group of the substrate. The protonated His^{33} would stabilize by a salt bridge successively Cys^{31} and Cys^{34} thiolates. In the second step, Cys^{34} thiolate would attack the Cys^{31} sulfur atom involved in the disulfide bond, causing the rupture of the latter. At the same time, the imidazole group in the oxidized Dtrx being deprotonated (pK_a 4.6), we propose that the thiolate of the reduced substrate would attack His^{33} and induce the release of the products of the reaction, an oxidized enzyme with deprotonated His^{33} and a reduced dithiol substrate.

As for all thioredoxins, this mechanism is reversible. DsbA contains the same CPHC sequence motif, but no data are available on the pK_a values for the imidazole group of this protein. We suggest that the protonation state could be identical to Dtrx. In DsbA catalysis, the two-step bimolecular nucleophilic substitution mechanism described in the literature (34) can be completed by a first step substrate activation. In this case, the imidazole group of histidine being deprotonated (pK_a 4.6) attacks the thiol group of the reduced substrate and induces the activation of the substrate with the formation of a thiolate cysteine. Effectively, in *E. coli*, it is unlikely that all of the 300 potential DsbA substrates present reactive cysteines (low pK_a). They most likely have to be activated by the deprotonated active site histidine of DsbA. In DsbA, mutations of the histidine located at the active site, diminished drastically the oxidase activity affecting the destabilization of the oxidized form of the enzyme (28, 35). According to the authors, the mutation affects the destabilization of the oxidized form of the enzyme. We think that the histidine mutant will affect not only the stability of disulfide bond but especially the activation of the substrates.

In conclusion, the new thioredoxin Dtrx from anaerobe *D. vulgaris* Hildenborough presents several unusual structural

Downloaded from http://www.jbc.org/ at CNRS on December 12, 2018

features and contains a particular active site consensus sequence, CPHC, which gives oxidizing properties. Our data suggest a particular specificity for its substrates, and one cannot exclude that this specificity may be limited to one of the gene products of the operon it belongs to. Further studies of these gene products will be essential to determine the physiological function of Dtrx. The knowledge of the protonation state for the residues involved in the reaction mechanism is highly important, and the pK_a values for all residues of the protein were determined for the first time. pK_a value determination allowed us to define the important function of the histidine residue at the catalytic site. Genome analysis of many bacteria reveals unusual thioredoxins. The structural and functional studies of such atypical systems will give new insights into TDOR catalytic mechanism.

Acknowledgments—We thank Dr. A. Dolla and Dr. B. Burlat for helpful discussions and Dr. P. Barré for critical reading of the manuscript.

REFERENCES

1. Holmgren, A., and Björnstedt, M. (1995) Thioredoxin and thioredoxin reductase. *Methods Enzymol.* **252,** 199–208
2. Rietsch, A., and Beckwith, J. (1998) The genetics of disulfide bond metabolism. *Annu. Rev. Genet* **32,** 163–184
3. Martin, J. L. (1995) Thioredoxin: a fold for all reasons. *Structure* **3,** 245–250
4. Mössner, E., Huber-Wunderlich, M., and Glockshuber, R. (1998) Characterization of *Escherichia coli* thioredoxin variants mimicking the active-sites of other thiol/disulfide oxidoreductases. *Protein Sci.* **7,** 1233–1244
5. Aslund, F., Berndt, K. D., and Holmgren, A. (1997) Redox potentials of glutaredoxins and other thiol-disulfide oxidoreductases of the thioredoxin superfamily determined by direct protein-protein redox equilibria. *J. Biol. Chem.* **272,** 30780–30786
6. Chambers, J. E., Tavender, T. J., Oka, O. B., Warwood, S., Knight, D., and Bulleid, N. J. (2010) The reduction potential of the active site disulfides of human protein disulfide isomerase limits oxidation of the enzyme by Ero1α. *J. Biol. Chem.* **285,** 29200–29207
7. Kersteen, E. A., and Raines, R. T. (2003) Catalysis of protein folding by protein disulfide isomerase and small-molecule mimics. *Antioxid. Redox Signal.* **5,** 413–424
8. Quan, S., Schneider, I., Pan, J., Von Hacht, A., and Bardwell, J. C. (2007) The *CXXC* motif is more than a redox rheostat. *J. Biol. Chem.* **282,** 28823–28833
9. Capitani, G., Rossmann, R., Sargent, D. F., Grütter, M. G., Richmond, T. J., and Hennecke, H. (2001) Structure of the soluble domain of a membrane-anchored thioredoxin-like protein from *Bradyrhizobium japonicum* reveals unusual properties. *J. Mol. Biol.* **311,** 1037–1048
10. Holmgren, A. (1985) Thioredoxin. *Annu. Rev. Biochem.* **54,** 237–271
11. Jeng, M. F., Holmgren, A., and Dyson, H. J. (1995) Proton sharing between cysteine thiols in *Escherichia coli* thioredoxin: implications for the mechanism of protein disulfide reduction. *Biochemistry* **34,** 10101–10105
12. Carvalho, A. T., Swart, M., van Stralen, J. N., Fernandes, P. A., Ramos, M. J., and Bickelhaupt, F. M. (2008) Mechanism of thioredoxin-catalyzed disulfide reduction: activation of the buried thiol and role of the variable active-site residues. *J. Phys. Chem. B* **112,** 2511–2523
13. Roos, G., Foloppe, N., Van Laer, K., Wyns, L., Nilsson, L., Geerlings, P., and Messens, J. (2009) How thioredoxin dissociates its mixed disulfide. *PLoS Comput. Biol.* **5,** e1000461
14. Pieulle, L., Stocker, P., Vinay, M., Nouailler, M., Vita, N., Brasseur, G., Garcin, E., Sebban-Kreuzer, C., and Dolla, A. (2011) Study of the thiol/disulfide redox systems of the anaerobe *Desulfovibrio vulgaris* points out pyruvate:ferredoxin oxidoreductase as a new target for thioredoxin 1. *J. Biol. Chem.* **286,** 7812–7821
15. Garcin, E. B., Bornet, O., Pieulle, L., Guerlesquin, F., and Sebban-Kreuzer, C. (2010) ^{1}H, ^{13}C and ^{15}N backbone and side-chain chemical shift assignments for oxidized and reduced desulfothioredoxin. *Biomol. NMR Assign.* **4,** 135–137
16. Holmgren, A. (1979) Thioredoxin catalyzes the reduction of insulin disulfides by dithiothreitol and dihydrolipoamide. *J. Biol. Chem.* **254,** 9627–9632
17. Hillson, D. A., Lambert, N., and Freedman, R. B. (1984) Formation and isomerization of disulfide bonds in proteins: protein disulfide-isomerase. *Methods Enzymol.* **107,** 281–294
18. Bertini, I., Felli, I. C., Gonnelli, L., Pierattelli, R., Spyranti, Z., and Spyroulias, G. A. (2006) Mapping protein-protein interaction by ^{13}C-detected heteronuclear NMR spectroscopy. *J. Biomol. NMR* **36,** 111–122
19. Jeng, M. F., and Dyson, H. J. (1996) Direct measurement of the aspartic acid 26 pKa for reduced *Escherichia coli* thioredoxin by 13C NMR. *Biochemistry* **35,** 1–6
20. Keller, R. L. J. (2004) Computer aided resonance assignment tutorial. *Cantina*
21. Cornilescu, G., Delaglio, F., and Bax, A. (1999) Protein backbone angle restraints from searching a database for chemical shift and sequence homology. *J. Biomol. NMR* **13,** 289–302
22. Shouldice, S. R., Cho, S. H., Boyd, D., Heras, B., Eser, M., Beckwith, J., Riggs, P., Martin, J. L., and Berkmen, M. (2010) *In vivo* oxidative protein folding can be facilitated by oxidation-reduction cycling. *Mol. Microbiol.* **75,** 13–28
23. Xu, Y., Yasin, A., Tang, R., Scharer, J. M., Moo-Young, M., and Chou, C. P. (2008) Heterologous expression of lipase in *Escherichia coli* is limited by folding and disulfide bond formation. *Appl. Microbiol. Biotechnol.* **81,** 79–87
24. Rinaldi, F. C., Meza, A. N., and Guimarães, B. G. (2009) Structural and biochemical characterization of *Xylella fastidiosa* DsbA family members: new insights into the enzyme-substrate interaction. *Biochemistry* **48,** 3508–3518
25. Krause, G., Lundström, J., Barea, J. L., Pueyo de la Cuesta, C., and Holmgren, A. (1991) Mimicking the active site of protein disulfide-isomerase by substitution of proline 34 in *Escherichia coli* thioredoxin. *J. Biol. Chem.* **266,** 9494–9500
26. Wunderlich, M., and Glockshuber, R. (1993) Redox properties of protein disulfide isomerase (DsbA) from *Escherichia coli*. *Protein Sci.* **2,** 717–726
27. Lundström, J., and Holmgren, A. (1993) Determination of the reduction-oxidation potential of the thioredoxin-like domains of protein disulfide-isomerase from the equilibrium with glutathione and thioredoxin. *Biochemistry* **32,** 6649–6655
28. Grauschopf, U., Winther, J. R., Korber, P., Zander, T., Dallinger, P., and Bardwell, J. C. (1995) Why is DsbA such an oxidizing disulfide catalyst? *Cell* **83,** 947–955
29. Ladenstein, R., and Ren, B. (2006) Protein disulfides and protein disulfide oxidoreductases in hyperthermophiles. *FEBS J.* **273,** 4170–4185
30. Fernandes, A. P., and Holmgren, A. (2004) Glutaredoxins: glutathione-dependent redox enzymes with functions far beyond a simple thioredoxin backup system. *Antioxid. Redox. Signal.* **6,** 63–74
31. Huber, D., Cha, M. I., Debarbieux, L., Planson, A. G., Cruz, N., López, G., Tasayco, M. L., Chaffotte, A., and Beckwith, J. (2005) A selection for mutants that interfere with folding of *Escherichia coli* thioredoxin-1 in vivo. *Proc. Natl. Acad. Sci. U.S.A.* **102,** 18872–18877
32. Chivers, P. T., and Raines, R. T. (1997) General acid/base catalysis in the active site of *Escherichia coli* thioredoxin. *Biochemistry* **36,** 15810–15816
33. Carvalho, A. T., Fernandes, P. A., and Ramos, M. J. (2006) Determination of the DeltapKa between the active site cysteines of thioredoxin and DsbA. *J. Comput. Chem.* **27,** 966–975
34. Kadokura, H., and Beckwith, J. (2010) Mechanisms of oxidative protein folding in the bacterial cell envelope. *Antioxid. Redox Signal.* **13,** 1231–1246
35. Guddat, L. W., Bardwell, J. C., Glockshuber, R., Huber-Wunderlich, M., Zander, T., and Martin, J. L. (1997) Structural analysis of three His32 mutants of DsbA: support for an electrostatic role of His32 in DsbA stability. *Protein Sci.* **6,** 1893–1900

Downloaded from http://www.jbc.org/ at CNRS on December 12, 2018

Structural and Mechanistic Insights into Unusual Thiol Disulfide Oxidoreductase

Edwige B. Garcin, Olivier Bornet, Latifa Elantak, Nicolas Vita, Laetitia Pieulle, Françoise Guerlesquin and Corinne Sebban-Kreuzer

J. Biol. Chem. 2012, 287:1688-1697.
doi: 10.1074/jbc.M111.288316 originally published online November 28, 2011

Access the most updated version of this article at doi: 10.1074/jbc.M111.288316

Alerts:
- When this article is cited
- When a correction for this article is posted

Click here to choose from all of JBC's e-mail alerts

Supplemental material:
http://www.jbc.org/content/suppl/2011/11/28/M111.288316.DC1

This article cites 34 references, 7 of which can be accessed free at
http://www.jbc.org/content/287/3/1688.full.html#ref-list-1

Downloaded from http://www.jbc.org/ at CNRS on December 12, 2018

Structural and mechanistic insights into an unusual thiol disulfide oxidoreductase

Edwige B. Garcin, Olivier Bornet, Latifa Elantak, Nicolas Vita, Laetitia Pieulle, Françoise Guerlesquin and Corinne Sebban-Kreuzer

Table of contents

Table S1: NMR and refinement statistics for Dtrx structures. S-2

Figure S1: Scrambled RNaseA (ScRNase) refolding assay: the cleavage of RNA by RNaseA was followed by 1D ^{1}H-NMR. S-3

Figure S2: Titration of the redox potential of the disulfide bond of Dtrx. S-4

Figure S3: pKa of ionisable residues of reduced and oxidized Dtrx. S-5

Figure S4: Superimposition of ^{1}H,^{15}N-HSQC spectra of Dtrx and DtrxH33G S-6

Figure S5: Solution structures of the reduced and oxidized forms of Dtrx S-7

Figure S6: Structural comparisons. S-8

Table S1: NMR and refinement statistics for Dtrx structures. Structural statistics and restraint violations of the 20 selected structures representative of Dtrx in solution at pH 5.7 and 290K.

	Reduced	Oxidized
NMR distance and dihedral constraints Distance constraints		
Effective distance restraints	1846	2108
Short range ($\|i-j\| \leq 1$)	1152	1261
Medium range ($1 < \|i-j\| < 5$)	276	415
Long range ($\|i-j\| \geq 5$)	418	432
Average number of restraints per residue	17	19
H-bond restraints	48	70
Dihedral angle restraints from TALOS	156	156
Structures statistics		
Restraint violations		
Distance >0,5Å	0	1
Dihedral >5°	0	5
Energies (kcal/mol)		
E_{total}	-2951	-2853
E_{bond}	58	57
E_{angle}	338	349
$E_{dihedral}$	975	992
E_{VdW}	-850	-866
$E_{electric}$	-7713	-7090
Average ensemble RMSD (Å)		
Backbone	0.94±0.15	0.59±0.11
Heavy atoms	1.31±0.14	0.94±0.11
Deviations from idealized geometry		
bonds (Å)	0.0097	0.0100
angles (°)	2.465	2.441
Ramachandran plot (%)*		
Most favorable region	86.5	83.4
Additionally allowed region	13.2	16.3
Generously allowed region	0.2	0.3
Disallowed region	0.0	0.0

* calculated using PROCHECK v. 3.5.4

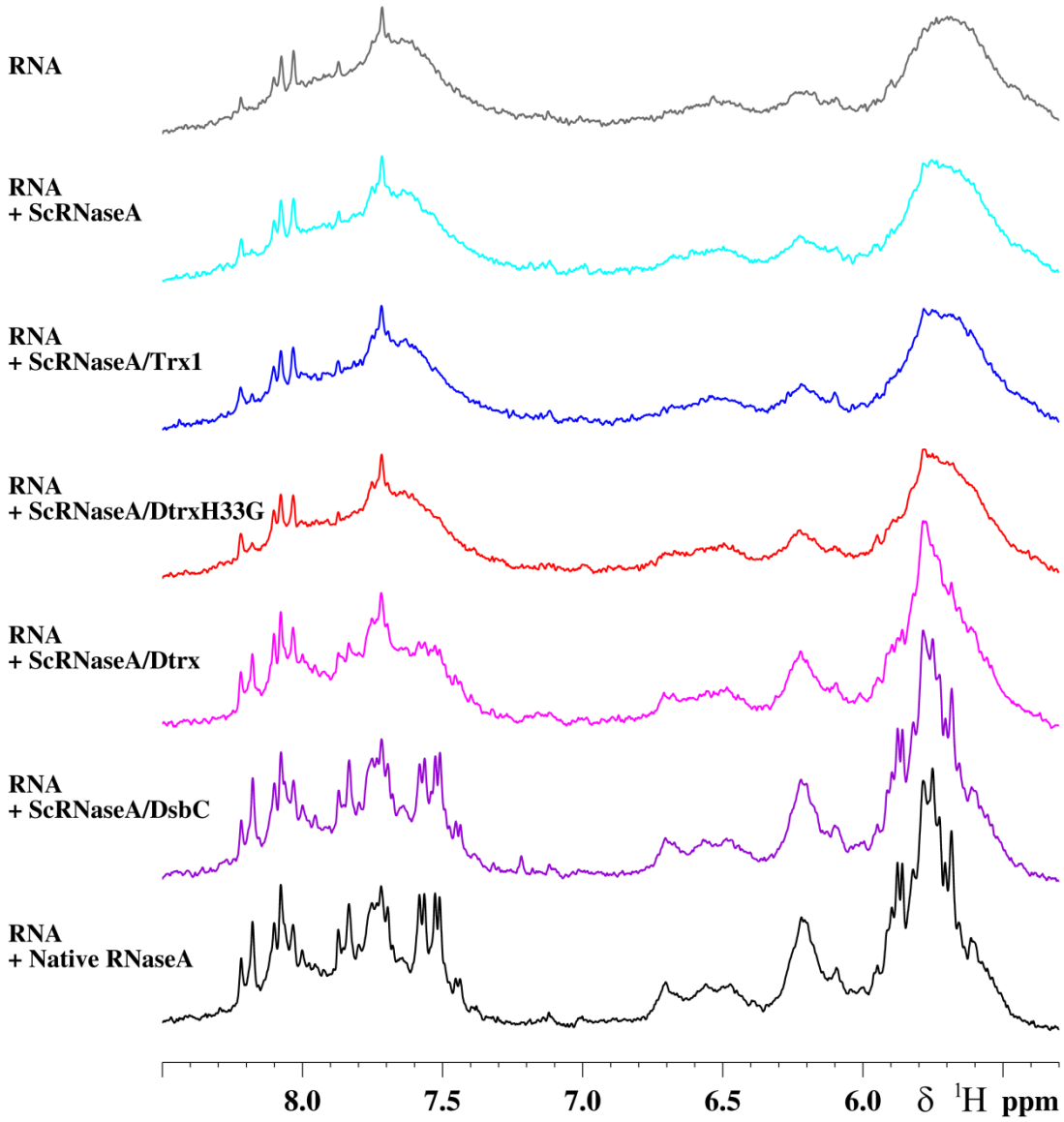

Figure S1: Scrambled RNaseA (ScRNase) refolding assay: the cleavage of RNA by RNaseA was followed by 1D ^{1}H-NMR.

1D 1H-NMR spectra of RNA with different mixture proteins: ScRNaseA (cyan), Trx1 and ScRNaseA (blue), DtrxH33G and ScRNaseA (red), Dtrx and ScRNaseA (pink), DsbC and ScRNaseA (purple), Native RNaseA (black). The assay was performed at 298K on a Bruker Avance III DRX 500 MHz spectrometer after 30 min of reaction. The NMR sample of RNA was 2 mg/ml in phosphate buffer 100 mM at pH 7 and 10 % D_2O. For the determination of the percentage of the RNaseA activity of native RNaseA and reshuffling of ScRNaseA after incubation with proteins, the mean intensity of several isolated peaks in RNA spectrum was used relative to RNA spectrum in the presence of native RNaseA. RNA spectrum (grey) in presence of scrambled RNaseA is used as blank.

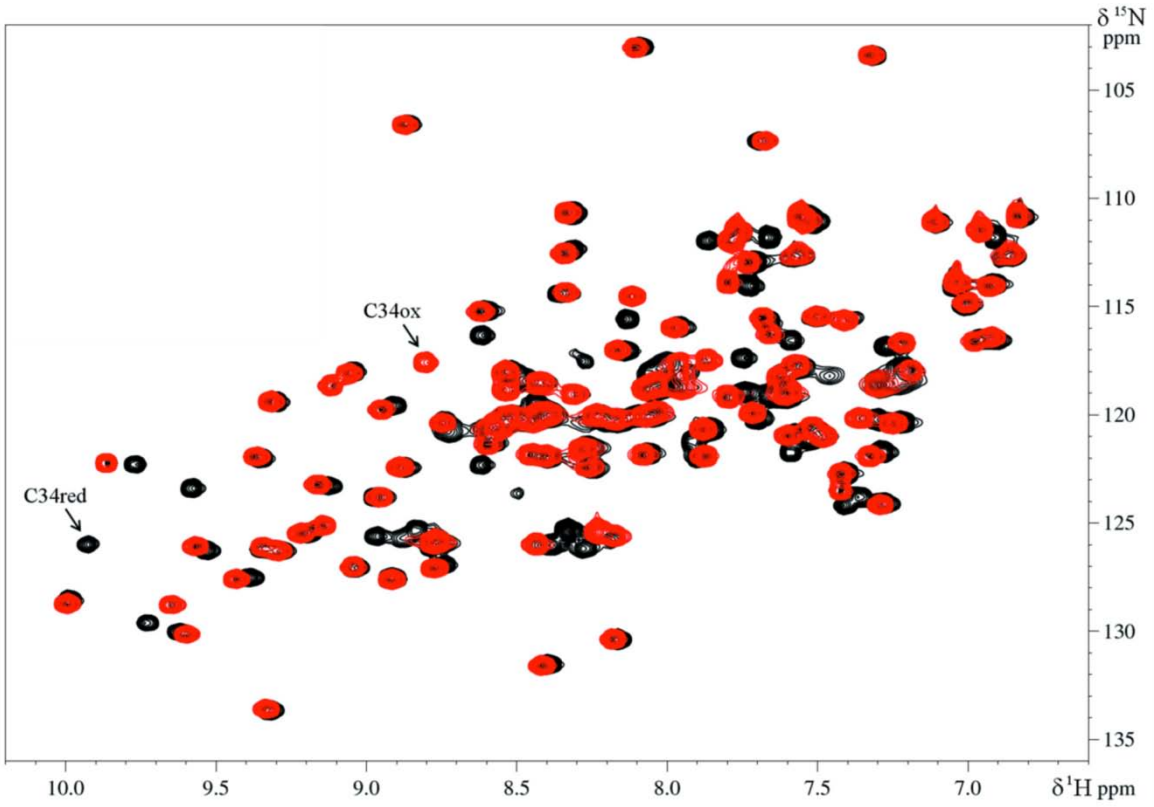

Figure S2: Titration of the redox potential of the disulfide bond of Dtrx. Superimposition of the ^{1}H-^{15}N HSQC spectra of Dtrx in the reduced (black) and oxidized (red) states at 298 K and pH 7. Arrows show the NH resonances of C34 under oxidizing (1.1 mM GSSG/1.8 mM GSH) and reducing (5.2 mM GSSG/23.6 mM GSH) conditions.

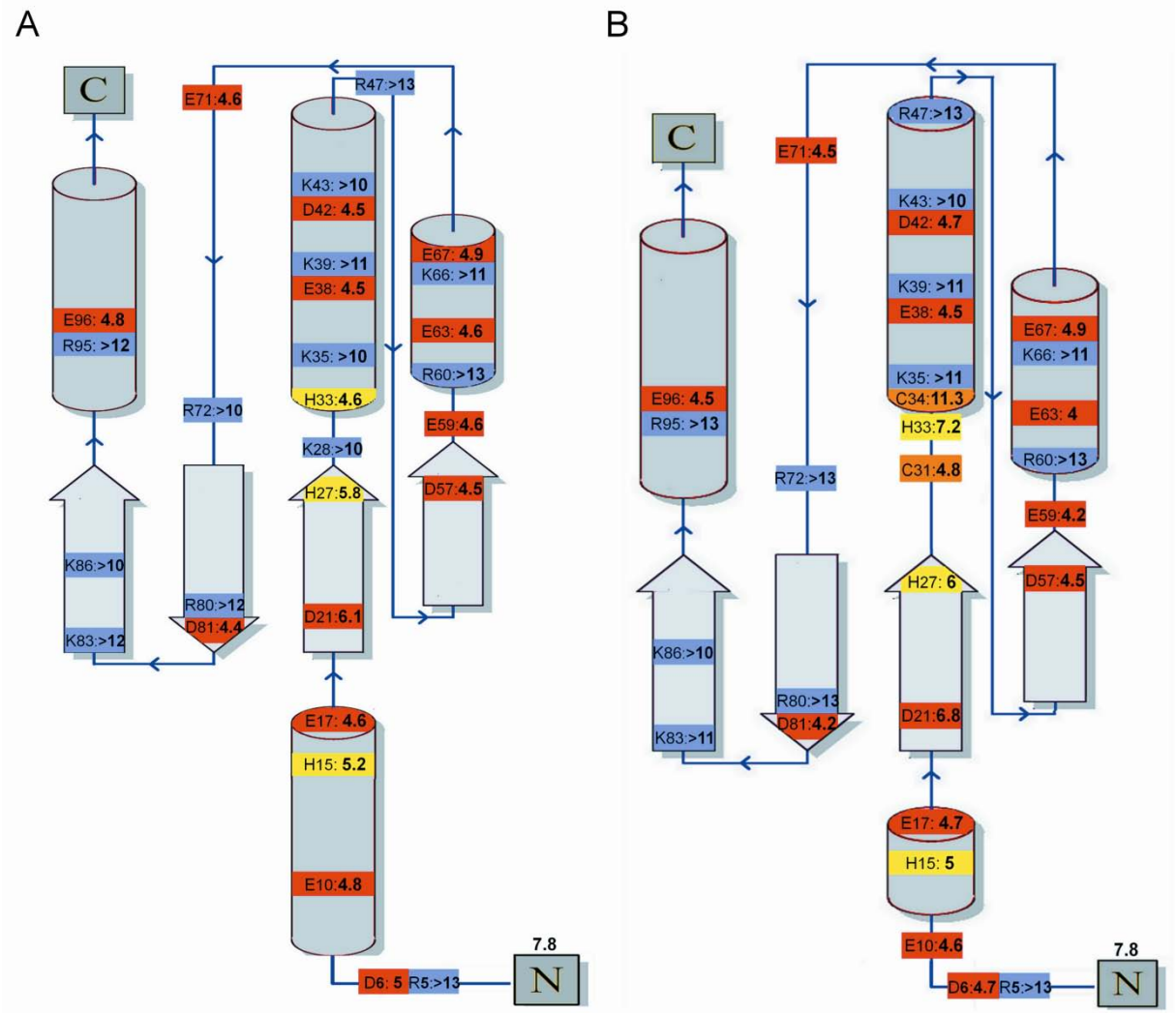

Figure S3: pKa of ionisable residues of reduced and oxidized Dtrx. Topology of the oxidized (A) and reduced (B) Dtrx forms. β-strands are shown as arrows and α-helices as cylinders. The pKas of ionisable residues determined by NMR are indicated. Acid residues Asp, Glu, are boxed in red, basic residues, Arg, Lys, are in blue, histidines are in yellow and cysteines are in orange.

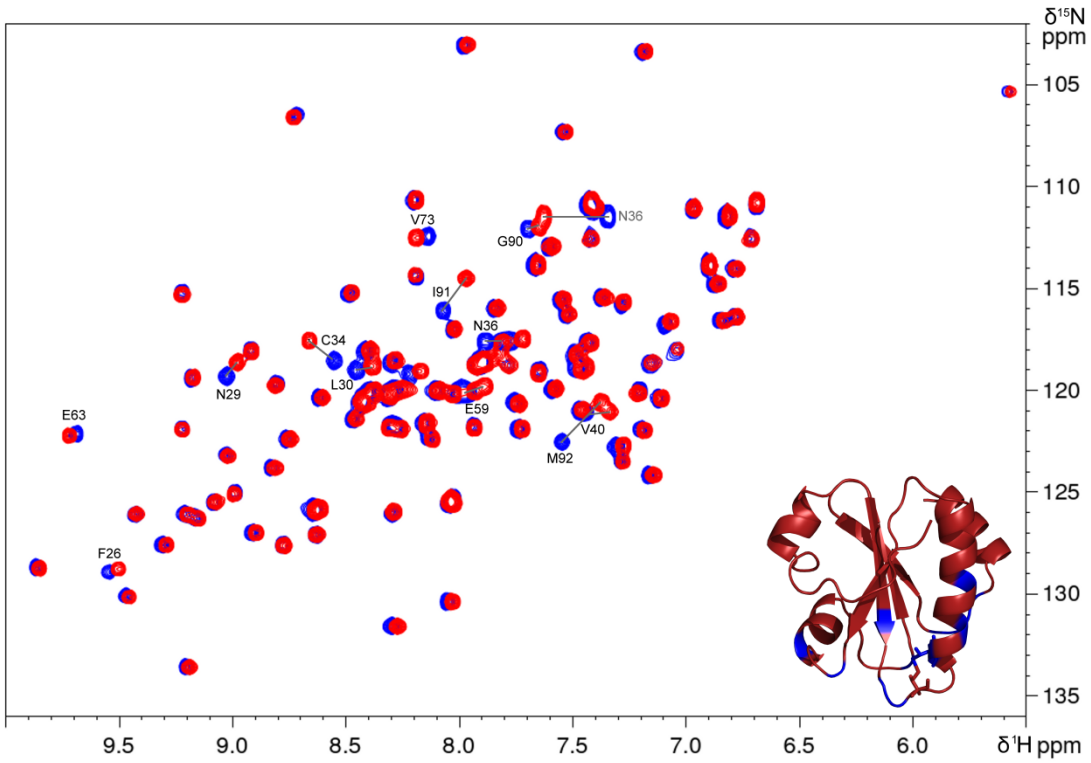

Figure S4: Superimposition of $^{1}H,^{15}N$-HSQC spectra of Dtrx and DtrxH33G. The samples were prepared in 100 mM potassium phosphate buffer pH 7, 50 mM NaCl. The spectra were recorded at 298 K on a 600 MHz NMR spectrometer. Residues undergoing chemical shift changes are labeled in the spectra and reported in blue on the Dtrx structure.

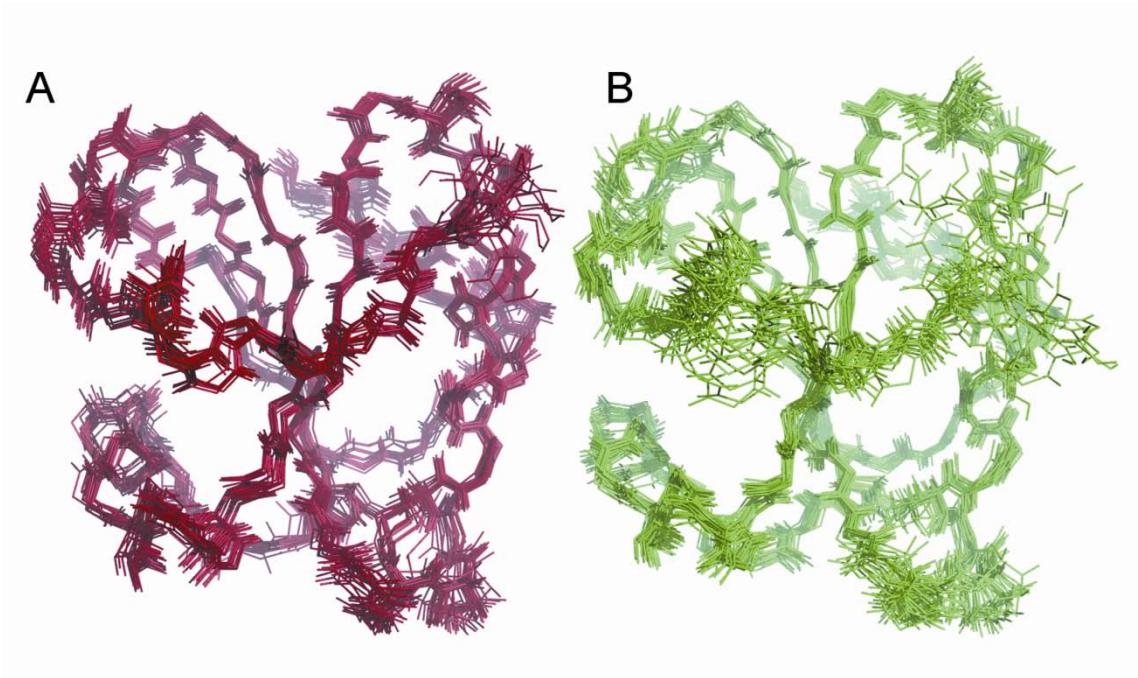

Figure S5: Solution structures of the reduced and oxidized forms of Dtrx. Superimposition of 20 representative structures of Dtrx in the oxidized (A) and reduced (B) states. The structures superimposed for minimal rmsd of all protein backbone atoms N, Cα and CO.

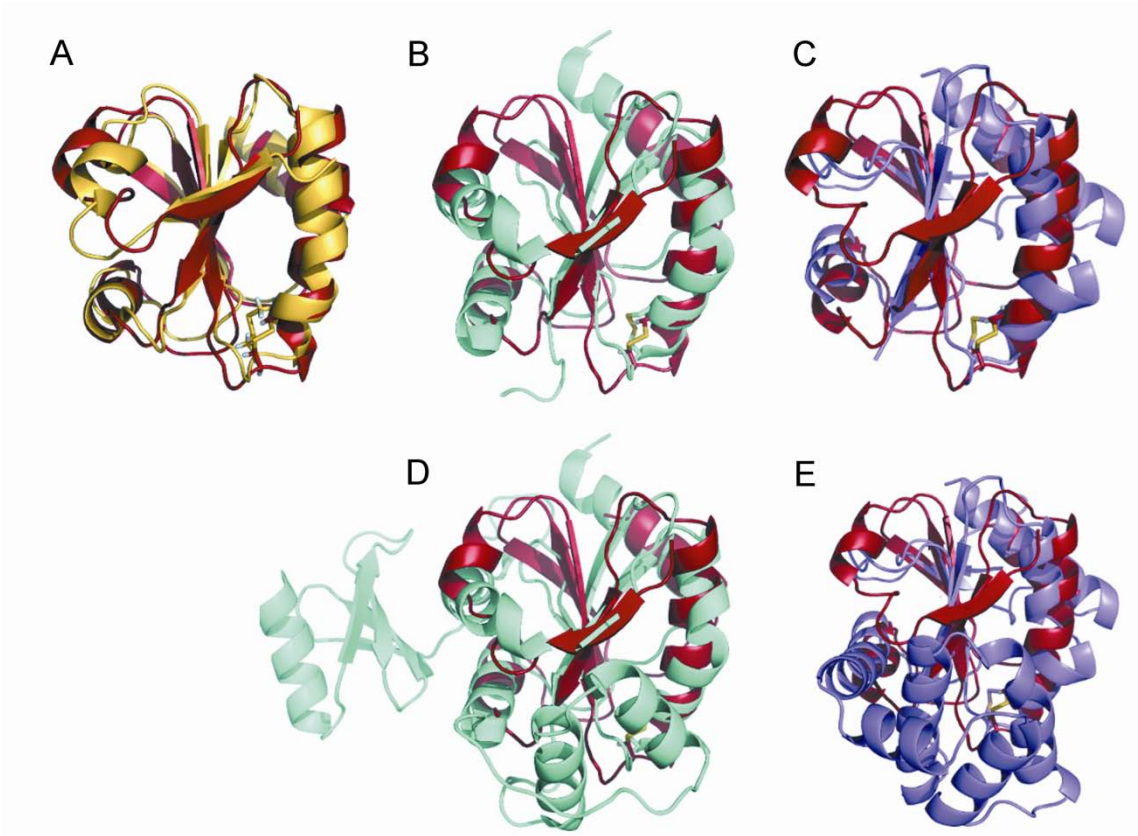

Figure S6: Structural comparisons. Overlay of the oxidized structures of Dtrx (red) with (A) *E. coli* Trx (yellow) (PDB entry 1XOA), (B) *E. coli* DsbA thioredoxin domain without the inserted helical domain F62-Q136 (blue) (PDB entry 1A2J), (C) *E. coli* DsbC thioredoxin domain without the inserted helical domain L126-V163 (purple) (PDB entry 1EEJ), (D) *E. coli* DsbA (blue), (E) *E. coli* DsbC (purple). The catalytic disulfide bond is shown as yellow sticks.